

Synthesis of a thin film of CuO/MgO/PVC nanocomposites for Photocatalytic applications

Nouhad Rouabah^{*a}, Roshan Nazir^{* b,c}, Yassine Djballah^d, AbQayoom Mir^e, Imene Ameur^f, Ouidad Beldjebli^f

a) *Laboratoire des Composants actifs et matériaux, Université Larbi Ben M'Hidi – Oum El Bouaghi*

b) *Department of Metallurgical and Materials Engineering Indian Institute of Technology Kharagpur, Kolkata - 721302, West Bengal.*

c) *Department of Chemistry Indian Institute of Technology Delhi, New Delhi 110016, India.*

d) *Physics Department, University of Batna 1, Algeria*

e) *Department of Chemistry Indian Institute of Technology, Ghandhinagar, 382355, India.*

f) *Université des frères Mentouri – Constantine 1, Algeria*

Received 16 October 2022; received in revised form 8 January 2023; accepted 10 February 2023 (DOI: 10.30495/IJC.2023.1970800.1968)

ABSTRACT

This study investigates the effect of a combination of copper and magnesium oxide nanoparticles embedded in a Polyvinyl chloride (PVC) matrix on photocatalytic activity. A thin film of CuO/MgO/PVC nanocomposites (NCs) was synthesized using the sol-gel route. Different weight percentages of CuO/MgO nanocomposites (5% and 15%) incorporated in the PVC matrix were deposited on glass strips using the spin coating method. The characterization of these thin films were carried out by a series of analytical and spectroscopic tools including PXRD, AFM, UV-Vis, and FTIR spectra analysis. The bandgap energy of MgO/PVC significantly reduced from 4.00 eV to 3.77 eV in 15% CuO/MgO/PVC NCs. This study also demonstrates the high ability of CuO/MgO/PVC thin films towards the photodegradation of methylene blue (MB) dye with a proposed reaction mechanism. A comparative analysis for the photodegradation of MB dye revealed superior photocatalysis by 15% with a rate constant of $5.20 \times 10^{-3} \text{ min}^{-1}$ showing about 44% efficiency. The credit goes to the decrease in the band gap, enhancement in charge separation, and increase in surface area of thin film CuO/MgO/PVC NCs.

Keywords: Polyvinyl chloride, Matrix, CuO/MgO Nanocomposites, Sol-gel, Photocatalysis.

1. Introduction

Dye and other toxic effluents from the textile industries need to be treated before being discharged into the water bodies. Dyes discharged from industries of paper, and textile are harmful, non-biodegradable organic molecules that pose threat to human and aquatic life. The past decade has paid extensive interest to getting rid of this environmental problem. However, these dyes are complex aromatic structures with pretty much stability that makes conventional biological treatment methods in effective, and non-destructive. Besides that, conventional biological treatment methods are costly as well. Photocatalysis has emerged as an effective way to treat this environmental issue.

The substrate/matrix role of organic polymers where the substantial dispersion of inorganic oxides results in the composite formation finds enormous applicability. The various fields where these heterostructures involving polymeric matrix find their applicability includes optoelectronics, automotive, aerospace, etc. Polymer composites have been found to be effective in dye degradation compared to other materials [1-6]. The properties of these Polymeric nanocomposites get affected by various factors like interfacial bonding, the embedding of nanoparticles, and the morphological behavior of the dispersed nanoparticles in the polymeric substrate[7-9].

Inorganic particles embedded in the polymer matrix have been found to increase the density, mechanical, magnetic and redox, electronic, and thermal, properties of the material. These properties depend on the shape,

*Corresponding author:

E-mail address: nouhadrouabeh@gmail.com (N. Rouabah); roshanandrabi@gmail.com (R. Nazir)

size, adhesion of particle/matrix interfaces, and filler content of the nanocomposites in the polymer matrix [10-13]. Metal oxide nanoparticles have been found to be effective for potential applications in photocatalysis. Among the various metal oxide nanoparticles, MgO nanoparticles have received tremendous research interest being less costly, abundant, thermally stable, biodegradable, and low toxicity. MgO has an FCC arrangement of the crystal lattice encompassing a band gap of 7.8 eV, which limits its use in photocatalysis applications. Researchers have doped MgO oxide with noble metals in order to reduce the band gap between the VB and CB with the aim to increase the photocatalytic nature of the material by shifting their absorption towards visible region wavelength [14-16]. The introduction of metal dopants in oxides also leads to the separation of electron-hole pairs thus encouraging charge transfer from the catalyst to the bulk solution. Amongst various metal dopants like Au, Ag, Pd, Cu, Pt, etc. Cu is a notable dopant and the credit goes to its activity, lower cost, high abundance, and stability [17,18]. Not only metal dopants but a combination of heterometal oxides have also played a significant and pivotal role in the separation of electron-hole pairs and enhanced photocatalytic activity.

In the present study, composites of CuO/MgO nanostructures were synthesized by utilizing a sol-gel approach. This CuO/MgO nanomaterial was embedded in the PVC substrate to get the nanocomposite of CuO/MgO/PVC with different weight percent of CuO/MgO (5% and 15%). The NCs of CuO/MgO/PVC were studied for photocatalytic dye (Methylene Blue) degradation and results were compared with pristine PVC and Cu/MgO. The nanocomposite materials were characterized by X-ray diffraction (XRD), FTIR, and Atomic Force Microscopy (AFM).

2. Experimental

2.1 Synthesis of Magnesium oxide (MgO) nanoparticles (NPs)

The MgO NPs were synthesized through the sol-gel technique. The precursor $Mg(NO_3)_2 \cdot 6H_2O$ was taken in C_2H_5OH and stirred for 24h, that results in white gel formation. After this, the separation of the mixture was performed by filtration, then washed with both ethanol and distilled solution. The mixture was dried for 24h at $100^\circ C$. The obtained powder was further annealed at $950^\circ C$ and then grinded to get the product of interest.

2.2 Synthesis of CuO/MgO NPs

A similar Sol-gel approach was utilized for the synthesis of CuO/MgONPs. Copper acetate, $Mg(NO_3)_2 \cdot 6H_2O$ and

$(COOH)_2 \cdot 2H_2O$ were used as precursor materials. The solutions of Copper acetate and $Mg(NO_3)_2 \cdot 6H_2O$ in ethanol (15mL) were obtained by dissolving and then subsequently stirring them. The above-prepared solutions were then amalgamated and a light blue clear solution was obtained, which was left for 20 minutes stirring. After that, the solution was kept uninterrupted for 12h. Then final product was filtered and washed with ethanol to remove any soluble impurities. The collected filtrate was kept in an oven for drying at $80^\circ C$ and then calcined at $500^\circ C$ for 2h at a heating rate of $10^\circ C/min$.

2.3 Preparation of CuO/MgO/PVC Nanocomposite.

1 g of PVC was added in 15 mL of THF under continuous stirring for 30 min. This results in the formation of a clear transparent viscous solution. To this solution, 0.5 g and 0.15g of already synthesized CuO/MgO nanoparticle powder was added under constant stirring for 1h that gives 5% CuO/MgO/PVC and 15% CuO/MgO/PVC polymer NCs. The thin films of the synthesized CuO/MgO/PVC polymer NCs on the glass support were obtained by spin-coating method.

2.3 Photocatalytic procedure

The photocatalytic activity of CuO/MgO/PVC nanocomposites were assessed towards the degradation of methylene blue dye in the presence of UV light. The photocatalytic degradation of MB dye in an aqueous solution was investigated under a UV light source (VL-215.LC, 15W, λ_{max} of 365 nm). A thin film of CuO/MgO/PVC nanocomposites coated on a glass slide (5×2.5 cm) was immersed in the beaker containing dye solution whose primary concentration was 10^{-5} mg/mL. The experiments were carried out in a photoreactor at RT and the sample was placed within a distance of 20 cm from the light source under constant stirring. Before carrying out the photocatalysis, the dye solution was kept in dark for a time duration of 30 minutes to ensure adsorption equilibrium. The experiments to determine the absorption values were carried out using the UV-Vis spectrometer (UV-1800 Shimadzu LC 2010-HT). In the presence of UV light, after every 30 minutes, the aliquots filled with the solution were used to determine the absorbance value, and the experiments were carried out for a total time of 150 minutes. The decrease in the intensity of the UV-Vis spectrum of MB dye during the photocatalysis reaction was noticed. The rate of degradation was calculated by the following formula; $Degradation (\%) = (1 - C_t/C_0) \times 100\%$ (1) Where C_0 and C_t represent the initial and final concentration of the dye respectively.

2.4 Materials and Devices

The materials synthesized above by the sol-gel technique were characterized by various techniques. The crystal structure was determined by PXRD using Cu K α radiation with 2 θ range from 10 $^\circ$ to 80 $^\circ$, at operating conditions of 40 kV voltage; operating current = 30 mA. The surface morphology was studied by AFM. AFM was done by employing a Nanoscope E Digital instrument with a silicon nitride cantilever in contact mode. The tip radius of the cantilever was 20 nm and the force constant was 0.56 N/m. The optical properties were studied by using UV/Vis absorption spectra of samples in the solid and liquid states using a UV-1800 Shimadzu LC 2010-HT spectrometer.

3. Results and Discussion

3.1 Structural study

3.1.1 X-ray diffraction (XRD) analysis

Fig. 1 shows the XRD structure of the pristine PVC, MgO/PVC, and CuO/MgO/PVC nanocomposites film with different CuO/MgO nanopowder loadings (5 and 15 wt%). For pure PVC thin film, its XRD shows a broadened hump, indicating their amorphous nature. The Bragg's reflections for MgO/PVC NCs at 2 θ =36.80 $^\circ$, 42.80 $^\circ$, 62.20 $^\circ$, 74.51 $^\circ$ and 78.37 $^\circ$ can be indexed to the (111), (200), (220), (311) and (222) crystal planes, which specifies typical cubic MgO phase (JCPDS:75-0447) [19,20]. However, additional peaks arise in CuO/MgO with 2 θ values of 35.51 $^\circ$, 38.68 $^\circ$, 48.60 $^\circ$, 62.10 $^\circ$, 66.31 $^\circ$ and 68.05 $^\circ$ corresponding to the diffraction planes of (002), (111), (-202), (220) and (-331) which specifies monoclinic CuO crystal phase (JCPDS: PDF#48-1548) [21]. The high intense peaks (002) and (111) crystal planes, confirms CuO NP exhibits a perfect crystalline structure. The slight shift in (111), (200), (220), (311), and (222) planes of MgO to the lower angle in the case of 5% CuO/MgO/PVC and 15% CuO/MgO/PVC as evident from **Table 1** clearly indicates a change in the crystal structure. This indicates the introduction of larger ionic radius Cu²⁺ ions (0.72 Å) have successfully substituted Mg²⁺ (0.65 Å) into the crystal lattice of the MgO. On the basis of Debye Scherer's formula (equation 1), the size of crystals were measured [22], and the values were calculated and recorded in **Table 1**.

$$D = 0.9\lambda/\beta\cos\theta \quad (1)$$

Where β = FWHM, θ is the diffraction angle, and λ is the X-ray wavelength (1.5405 Å). The calculated

average crystallites sizes (D) of MgO NPs in MgO/PVC is 30 nm, and the average size of CuO and MgO NPs in 5% CuO/MgO/PVC NCs and 15% CuO/MgO/PVC NCs is calculated approx. 9.29 and 15.13 nm respectively.

3.1.2 FTIR Analysis

The identification of various functional groups present in the samples were confirmed from the FTIR spectroscopy as shown in **Fig. 2**, (from 4000-400 cm⁻¹). Sharp peaks were observed in the films at 756 and 904 cm⁻¹, which correlates to the PVC Bond [23]. As the amounts of CuO/MgO is increased, a shift towards lower frequencies is perceived showing an effective interaction of CuO and MgO with C-Cl, C-H bonds of PVC matrix, a similar pattern was observed within XRD evaluation [24]. In the spectrum of MgO/PVC NCs, three distinctive bands at 615, 1324, 1434 cm⁻¹ indicates the bending vibrations of Mg-O-Mg, C-H, and C=C respectively [25]. The CuO/MgO/PVC nanocomposite film spectrum shows similar absorption peaks and none of the peak for CuO was present due to a smaller percentage of CuO. The presence of Mg-O and C=O vibrations clearly indicates the presence of these oxides in CuO/MgO/PVC. SEM images of 15% CuO/MgO/PVC is depicted in **Fig. 3** and from the figure, it is clear that the deposited film shows sheet-like morphology. EDX of the film was also taken (**Fig. 4**). From the EDX spectra substantial amount of Cu, Mg, O, C, and Cl is found.

3.2 Optical study

3.2.1 UV-Vis analysis

Optical properties of pure PVC, MgO/PVC, and CuO/MgO/PVC (5, 15 Wt%) NCs thin film were studied by using a double beam UV-Vis spectroscopy (**Fig. 5**). From the figure, it is observed that pure PVC is highly transparent (90%), while all the films exhibited strong absorption between 300 and 400 nm, and had a sharp absorption edge at 300 nm. The absorption bands around 364 and 398 nm may be due to the excitation of O₂⁻ anions in the edges and corners of MgO [26]. With an increase in the amount of CuO/MgO in these films from 5% to 15%, absorption decreases as shown in the inset of **Fig. 5**.

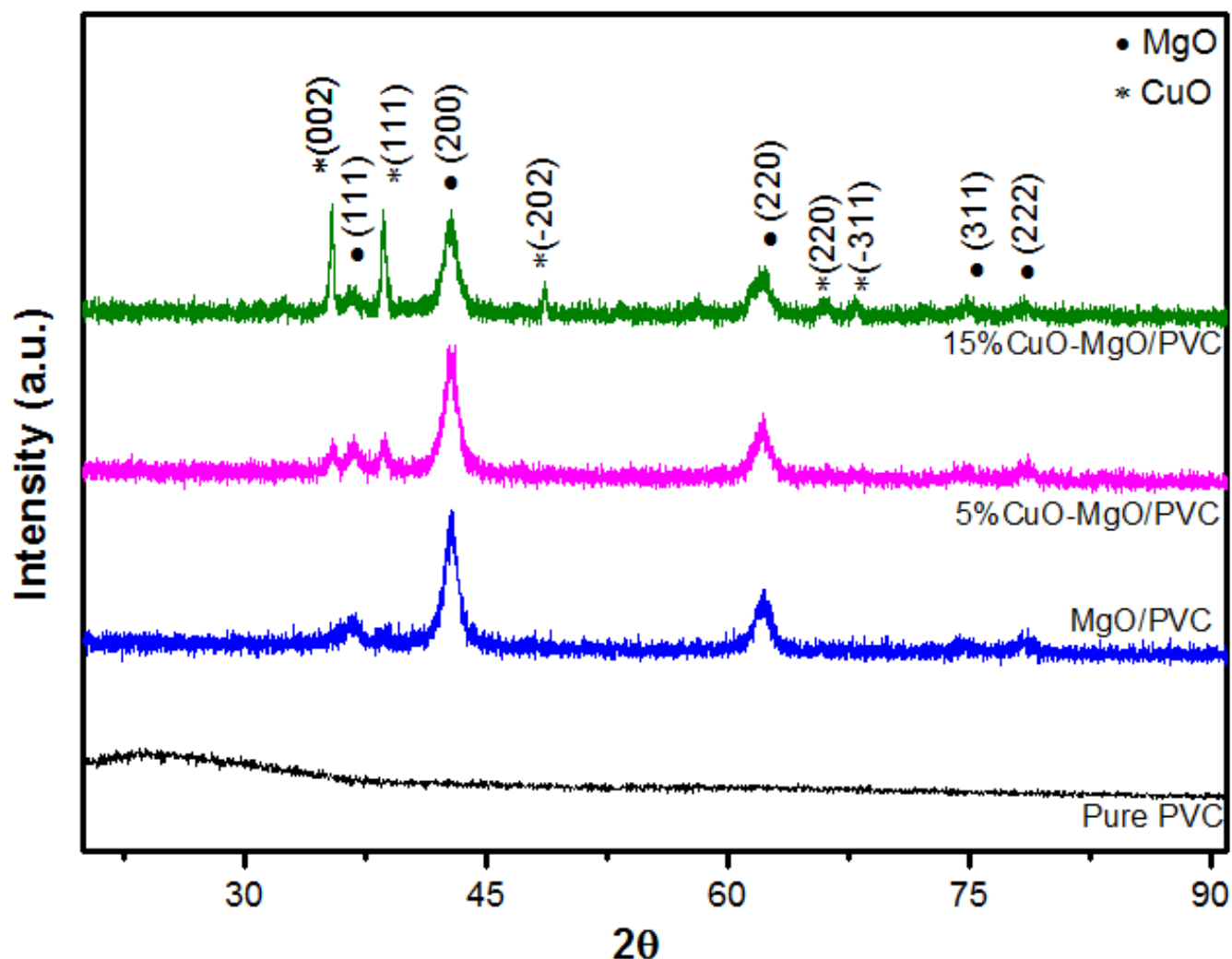


Fig 1. The XRD patterns of Pure PVC, MgO/PVC, and CuO-MgO/PVC nanostructures.

Table 1. Structural parameters of MgO/PVC and CuO-MgO/PVC nanocomposites thin films.

Samples	2θ(°)	(hkl)	FWMH(°)	d (nm)	D (nm)
MgO/PVC	36,8	(111)	1,5	5,60	6,71
	42,81	(200)	1,07	8,01	
	62,18	(220)	1,42	6,54	
5%CuO/MgO/PVC	35,43	(002)	0,62	13,50	9,29
	36,61	(111)	1,1	7,60	
	38,68	(111)	0,82	10,30	
	42,73	(200)	1,07	7,98	
	61,99	(220)	1,3	7,10	
15%CuO/MgO/PVC	35,59	(002)	0,32	26,1	15,13
	36,7	(111)	0,71	11,8	
	38,68	(111)	0,36	23,4	
	42,63	(200)	1,09	7,83	
	61,90	(220)	1,42	6,51	

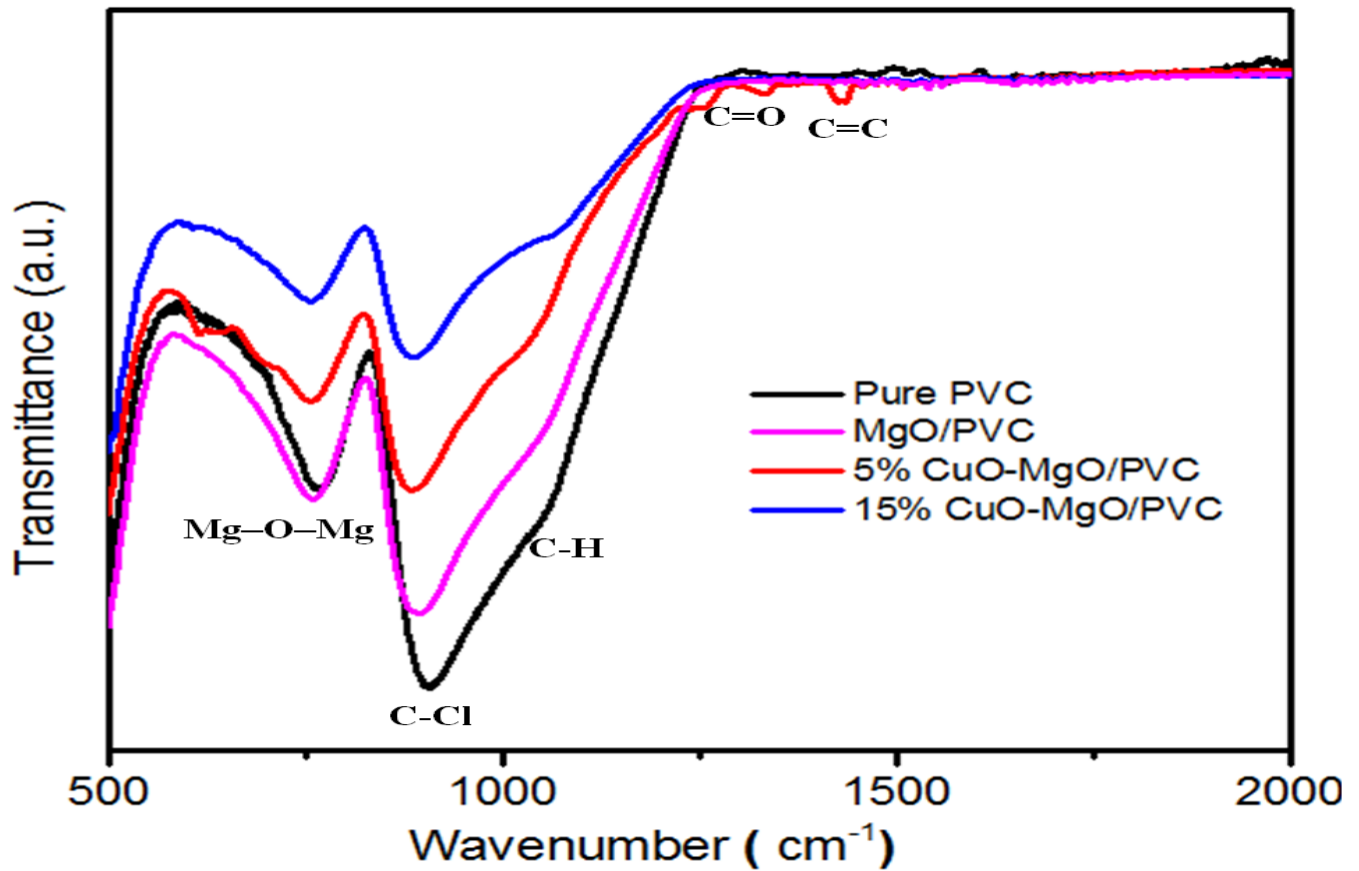


Fig 2. FTIR spectrum of PVC, PVC/MgO, and Cu-MgO/PVC nanocomposites.

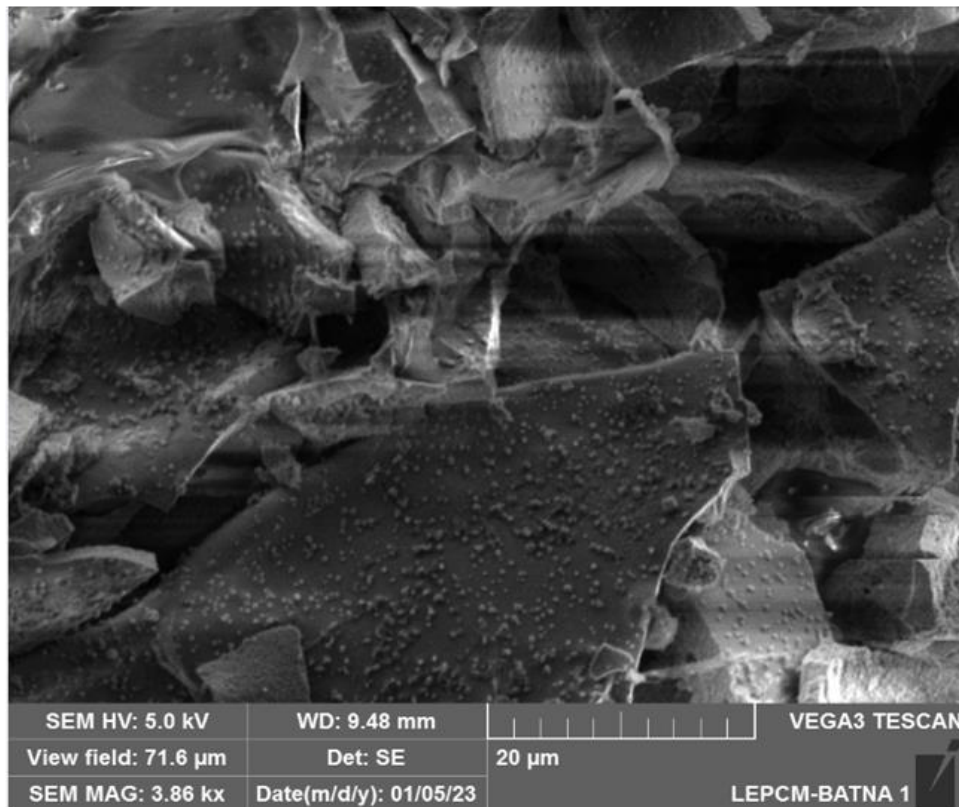
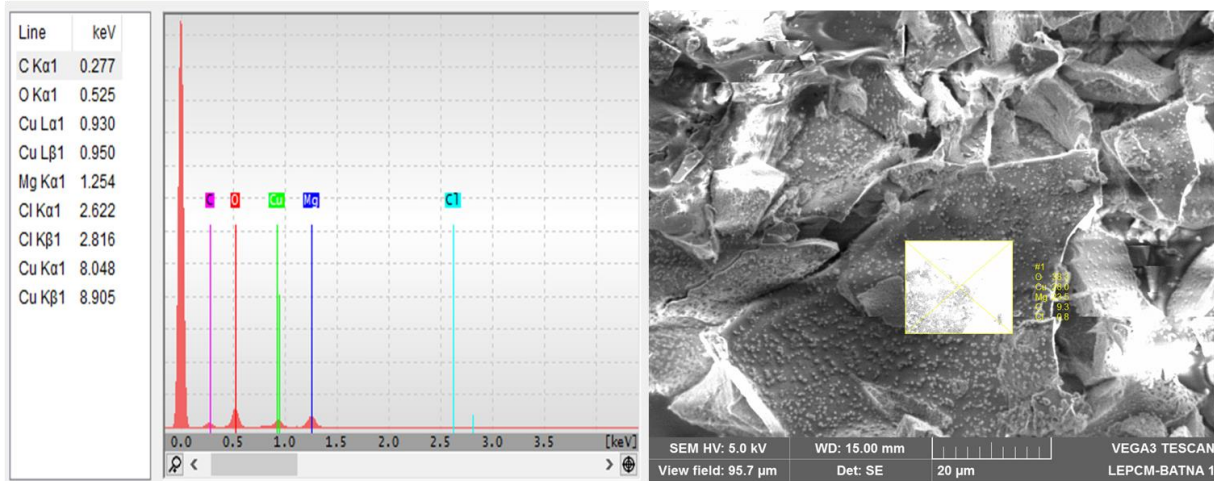


Fig 3. SEM image of 15% CuO/MgO/PVC NCs



Element	Unn. wt.%	Norm. wt.%
O	39.4	38.3
Cu	28.8	28.0
Mg	24.2	23.5
C	9.6	9.3
Cl	0.8	0.8

Fig 4. EDX spectra of 15% CuO/MgO/PVC NCs

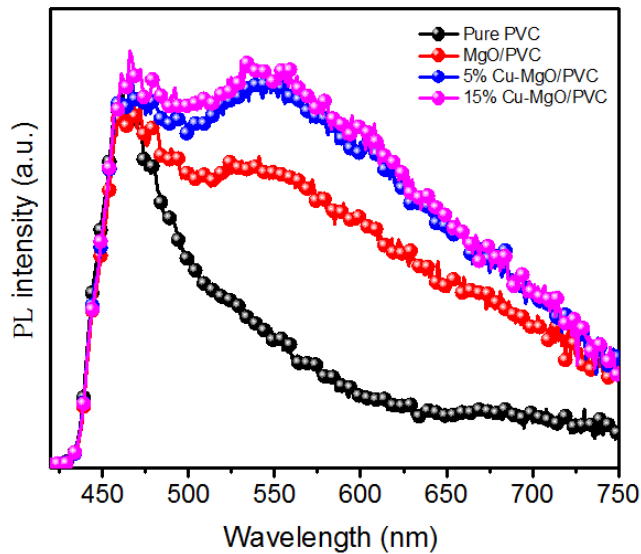


Fig. 5 Optical transmission spectra in the UV-Visible region of Pure PVC, MgO/PVC, and Cu-MgO/PVC nanocomposite thin films.

3.2.2 Determination of Optical Band

The band gaps were determined by employing diffused reflectance spectroscopy (DRS), the band gap of pure CuO and MgO is 1.8 eV and 5.2 eV respectively before contact as described in **Scheme 1**. The incorporation of p-type CuO in n-type MgO results in the creation of a p-n heterojunction. As described in **Scheme 1**, the E_f (fermi level) of MgO is shifted low while that of CuO is shifted

upward (after contact in **Scheme 1**) at equilibrium. The energy band gaps of the above-synthesized materials were calculated from the plot of $(\alpha h\nu)^{1/2}$ vs $(h\nu)$ in **Fig. 6**. It was observed that the increase in the % of CuO/MgO nanoparticles in the PVC matrix leads to the reduction of energy gap from ~4.00 eV for pure PVC to 3.77 eV. The reason behind this may be due to the defects formation accompanying the synthesis of CuO-MgO nanostructure [28]. This may be also credited to the change in band structure in CuO dopant MgO that may introduce new local levels in the conduction band, and thus encourage the electron transport from valance to conduct band [29].

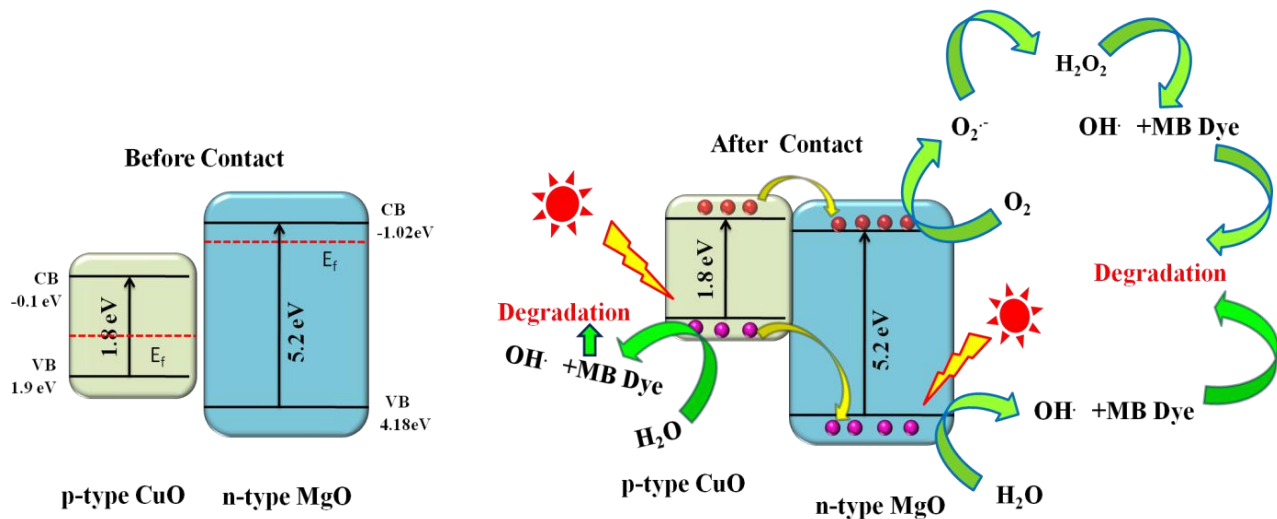
3.3 Morphological study

3.3.1 Atomic Force Microscopy (AFM) analysis

The AFM studies are used to identify the topography and the surface behavior of nanostructures. In AFM various digital images are obtained that give the quantitative measurements of various surface parameters, and the analysis of images from various aspects, including 3D simulation, as shown in **Table 2** [30]. **Fig. 7** shows the 2D and 3DAFM images of the surface topography of pure PVC, MgO/PVC, and CuO/MgO/PVC nanocomposites of varying contents. The AFM images of CuO/MgO/PVC NCs revealed the change in surface morphology of PVC with the dispersion of CuO/MgO in PVC. The Figures indicate that CuO/MgO/PVC possesses a highly porous structure

in comparison to MgO/PVC. The results thus clarify that CuO/MgO loading in PVC enhances the porosity, thus the specific surface area. The bright points on the surface of the film shows the growth of well-developed grains of MgO crystallites [31]. The images confirm the successful distribution of CuO/MgO nanoparticles into the polymer matrix. The average diameter of pores, the mean roughness (Ra), and root mean square roughness (Rq) parameters were measured for these nanostructures also as listed in **Table 2**. It is pertinent to mention here that the values mentioned in the table are average ones which showed an arithmetical variation, dependent on the position on samples where measurements were performed. These values showed a direct association

with the increment in CuO/MgO loadings. From **Table 2**, it is observed that Ravares from $1.933 \leq Ra \leq 7.901$, and the Rqlies in-between $4.12 \leq Rq \leq 10.075$. The RMS value elevates as CuO/MgO loading increases, specifying that CuO/MgO/PVCNCs films possess a greater irregular surface than MgO/PVC NC. Appropriately, 5% and 15% CuO/MgO/PVC NC films have the utmost eminent previous, prompting a substantial unambiguous surface state. Thus, the formation of porous configuration films is the most encouraging method to advance photocatalytic activity and reutilizing safety [32].



Scheme 1. Energy diagram representing p-n heterojunction of CuO/MgO nanocomposites, illustrating separation of electron-hole pairs and bandgap and their involvement in MB dye degradation

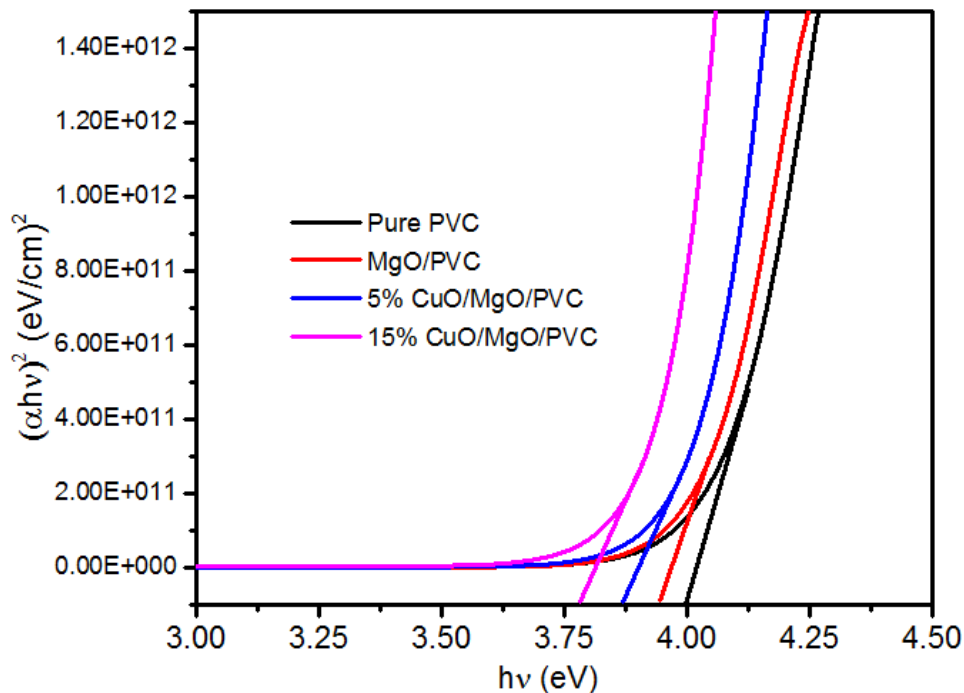


Fig. 6. The bandgap of various synthesized nanostructures.

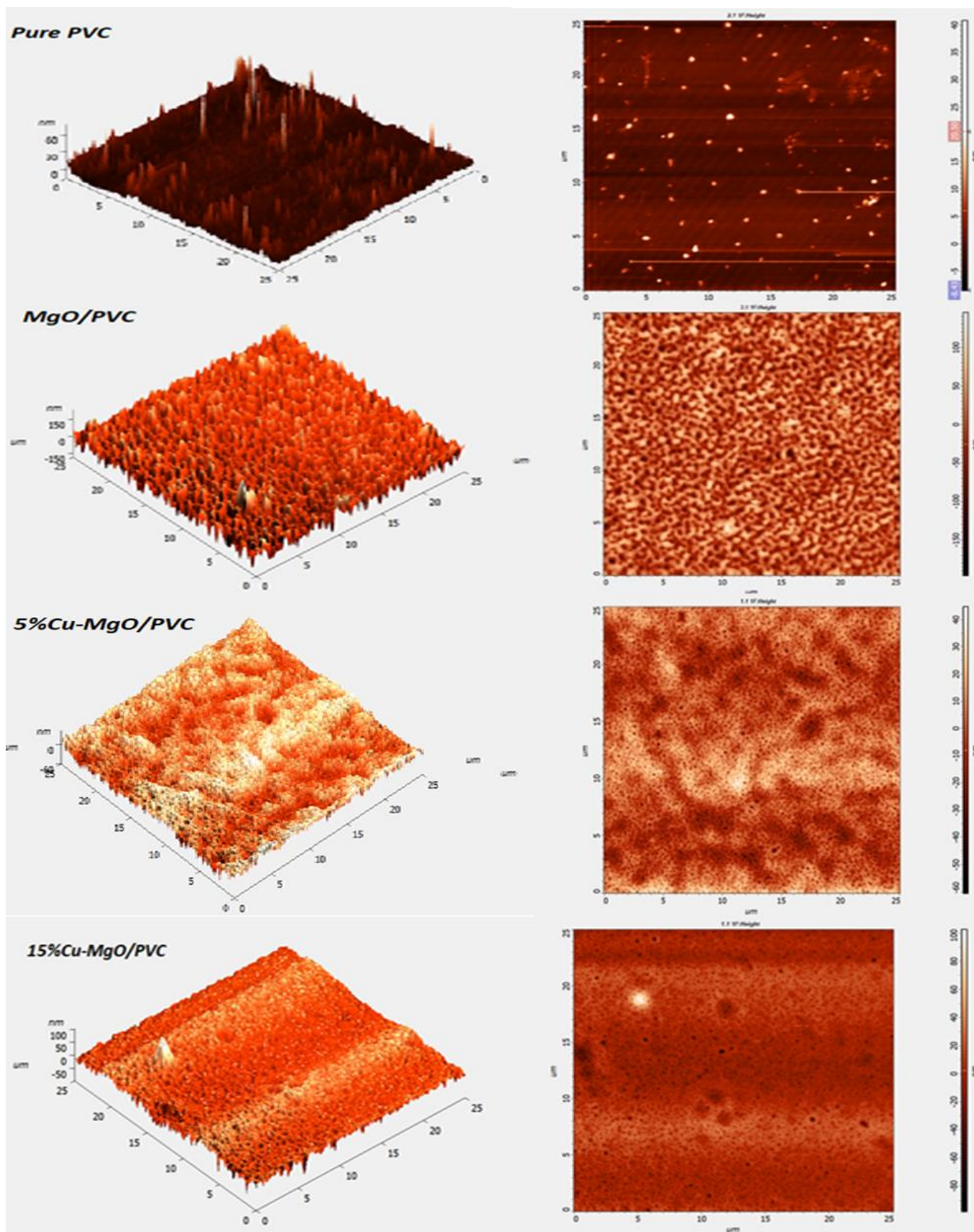


Fig.7: AFM for pure PVC, PVC/MgO, and Cu-MgO/PVC nanocomposites.

Table 2. The values of roughness average, the root mean square, and the diameter of pores of above-synthesized materials.

Samples	Avg. Diameter of pores	Roughness average	Root mean square
Pure PVC	36-360	1.93	4.12
MgO/PVC	31-500	3.407	4.23
5%CuO/MgO/PVC	25-500	6.213	7.304
15%CuO/MgO/PVC	12.5-375	7.901	10.075

3.4 Photocatalytic tests

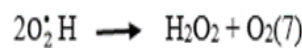
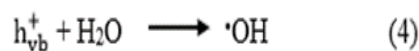
Fig. 8 Shows the degradation spectra of methylene blue dye by PVC pure, MgO/PVC, and CuO/MgO/PVC nanocomposite solutions under UV irradiation for 150 mins. The MB detoxification efficiency enhances on much exposure with time. The percentage of degradation of MB by these films were calculated using equation 2 [33]:

$$\% \text{ Degradation efficiency} = [(C_0 - C)/C_0] \times 100 \quad (2)$$

The symbols of C_0 and C demonstrate the initial and final concentration of MB solutions respectively. These are proportional to initial absorption and the absorption found after exposure to sunlight [34]. The highest activity was achieved for the 15% CuO/MgO/PVC nanocomposites while Comparing pure PVC and CuO/MgO/PVC. It was found that the degradation efficiency of 44% after 2h UV light irradiation can be because of the most efficient charge separation in CuO/MgO/PVC NCs that also increases the rate of electron transfer to dissolved oxygen. The reaction kinetics is an important parameter to study the rate of decomposition of toxic chemicals present in water. The kinetics ($\ln C/C_0$ vs t) of MB dye with PVC, MgO/PVC, and CuO/MgO/PVC NCs at different concentrations is shown in **Fig. 9**. The figure clearly reveals that there is a direct relation between the concentration and the time, thereby depicting the first order rate of reaction followed for the detoxification process. The rate constant (k) values given by the slopes of PVC, MgO/PVC, and (5%, 15%) CuO/MgO/PVC nanocomposites are $1.64 \times 10^{-3} \text{ min}^{-1}$, $2.13 \times 10^{-3} \text{ min}^{-1}$, $4.04 \times 10^{-3} \text{ min}^{-1}$, $5.20 \times 10^{-3} \text{ min}^{-1}$, respectively. The high value of k for CuO/MgO/PVC reveals its outstanding photocatalytic efficiency than pure PVC and MgO/PVC NCs. For the heterojunction CuO/MgO/PVC, the photocatalytic ability increases as the doping level are increased by 5-15%. The explicit reason for this is the enhancement of porous structure, which is accompanied by the concomitant elevation of active sites resulting in the excessive adsorption of dye molecules on the catalyst's surface. The formation of a heterojunction between CuO/MgO NPs and the PVC

matrix results in the reduction of bandgap enhances its absorption in the UV region leading to maximum electron-hole pair generation [35]. An increase in $\bullet\text{OH}$ and $\text{O}_2^{\bullet-}$ contents is observed as indicated in scheme 1 which thereby improves the efficiency of the photocatalyst. The higher generation of charge carriers results there more participation in the photo processes and hence the excess removal of toxic dyes [36].

The enhanced photoactivity results in CuO/MgO/PVC NCs are due to the reduction in the bandgap resulting in efficient light utilization. The better separation of photogenerated charge carriers in 15%CuO/MgO NCs promotes the process of interfacial electron transfer between CuO and MgO oxides [37]. It all happens, by exposing the surface of CuO/MgO NPs to UV light, which results in the excitation of electrons from the VB after the absorption of a certain specific wavelength leading to the creation of holes in the VB and electrons excess in CB. The excited electrons are supplied to oxygen species present in the water, which are responsible for producing reactive oxygen $\text{O}_2^{\bullet-}$ that leads to the formation of H_2O_2 , which further generates $\bullet\text{OH}$ that leads to degradation of organic dye in the aqueous medium. The holes in the valance band in an aqueous medium also generate hydroxyl radicals that also help in dye degradation. These reactive species of hydroxyl radicles, superoxide radicles, and hydrogen peroxide are responsible for the removal of organic pollutants from water [38]. The following equations explain the various reaction sequences of photocatalytic degradation :



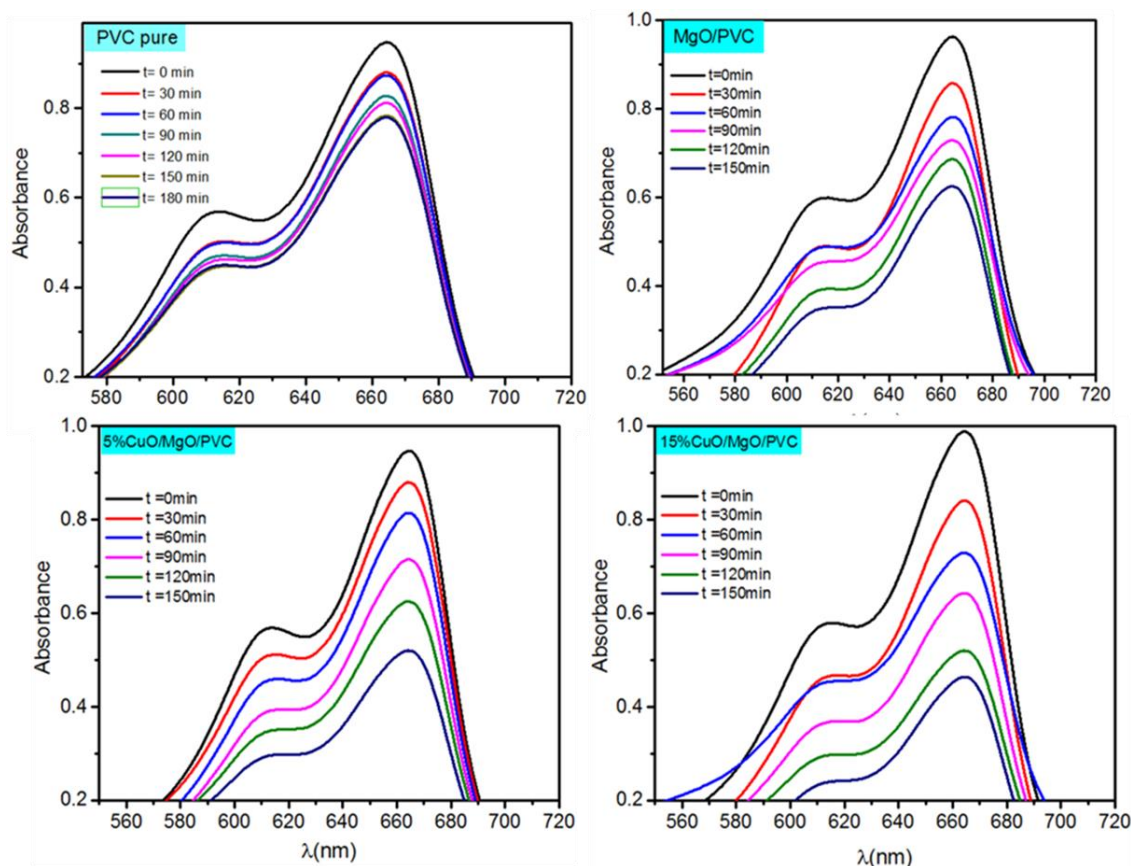


Fig. 8. Photocatalytic degradation of MB on exposing to UV light irradiation employing PVC; MgO/PVC and CuO-MgO/PVC heterostructure as catalysts.

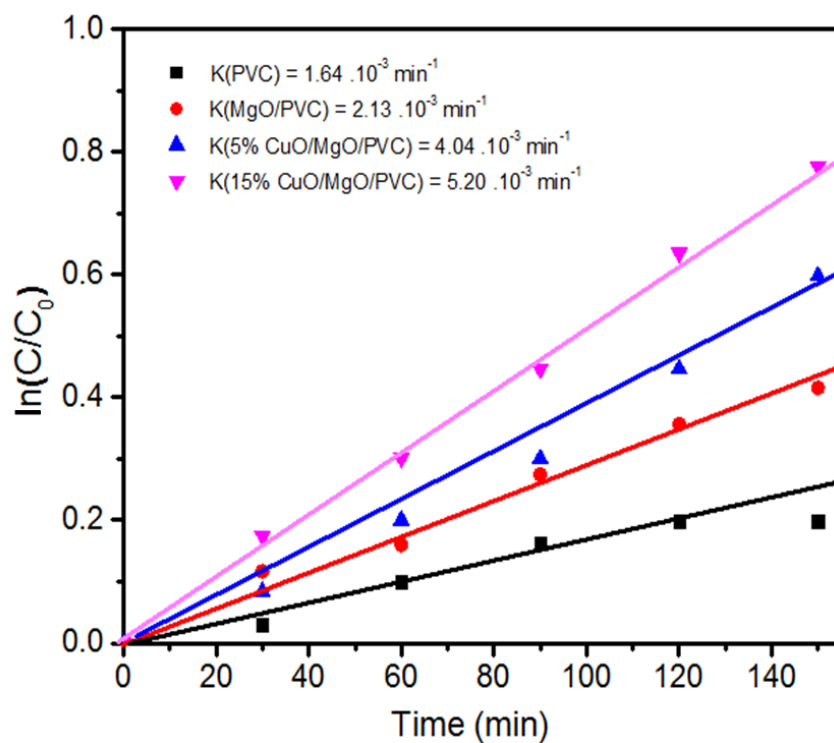


Fig. 9. Rate of dye disintegration under, $[\ln C/C_0]$ vs. time.

4. Conclusions

The degradation of MB dye by photocatalysis was studied in this report. The CuO and MgO nanoparticles were embedded into the PVC matrix to generate the photocatalyst CuO/MgO/PVC of different wt% (5%, 15%). Among the different wt%, 15% CuO/MgO/PVC catalyst showed better catalytic activity as compared to other catalysts studied here. The better catalytic activity of the 15% CuO/MgO/PVC is supported by a decrease in the band gap of the MgO/PVC with an increase in the % weight of CuO/MgO in the PVC matrix as evident from the UV-vis spectra. This increase in photocatalysis is because of better charge separation of charge carriers (holes and electrons). The better catalytic activity can be further explained by the high surface area/roughness of the most efficient catalyst as evident from the AFM analysis images. The study, therefore, confirms that the composite formation between CuO and MgO and their deposition in the polymer matrix resulted in enhanced photocatalytic activity, because of the synergistic effect between the composites and the matrix. The study thus provides new insights about the development of the such type of catalysts for their use in various catalytic performances.

Acknowledgements

This research was funded by Princess Nourah bint Abdulrahman University Researchers Supporting Project Number (PNURSP2022R42), Princess Nourah bint Abdulrahman University, Riyadh, Saudi Arabia. Also, the author Dr. AbuAlnaja appreciated Taif University Researchers Supporting Project number (TURSP-2020/267), Taif University, Taif, Saudi Arabia.

Declaration of Competing Interest:

In this report, the authors declare no financial interests or personal relationships.

Author Contributions

NR performed all the experimental work, collected and analyzed the data, and wrote the first draft of the manuscript. RN commented on the manuscript and approved the final version of the manuscript. AQM revised the manuscript and approved the final version of the manuscript. RN and NR conceptualized and designed the work.

References

[1] G. A. Rather, A. Nanda, M. A. Pandit, S. Yahya, M. A. Sofi, H. Barabadi, M. Saravanan, *Inorg. Chem. Commun.* 134, (2021) 109020

[2] B. Srinivas, M. A. Pandit, K. Muralidharan, *ACS Omega*, 4, (2019) 14970–14980

[3] A. Joseph, S. Billakanti, M. A. Pandit, S. Khatun, A. K. Rengan, K. Muralidharan, *Environ. Sci. Pollution Research*. 29, (2022) 56863-56875

[4] M. A. Pandit, S. Billakanti, K. Muralidharan, *J. Environ. Chem. Eng.* 8, (2020) 103542.

[5] M. A. Pandit, D. S. H. Kumar, S. Billakanti, M. Ramadoss, K. Muralidharan, *J. Phys. Chem. C*, 124, (2020) 18010-18019

[6] T. Linda, S. Muthupoongodi, X. Sahaya Shajan, S. Balakumar, *J. Mat. Sci. Forum* 807, (2015) 91-99.

[7] G. Momen, M. Farzaneh, *Rev. Adv. Mater. Sci.* 27, (2011) 1-13.

[8] I. Y. Jeon, J. B. Baek, *Materials* 3, (2010) 3654-3674

[9] S. F. Bdewi, O. Gh. Abdullah, B. K. Aziz, A. A. R. Mutar, *J. Inorg. Organomet. Polym.* 26, (2016) 326-334

[10] P. Sokhandani, A. A. Babaluo, M. Rezaei, M. Shahrezaei, A. Hasanzadeh, S. G. Mehmamdoost, R. Mehdizadeh, *J. Appl. Polym. Sci.* (2013) 3265-3272

[11] M. Hojamberdiev, Z. C. Kadirova, S. S. Daminova, K. Yubuta, H. R. Khosroshahi, K. T. Sharipov, M. Miyauchi, K. Teshima, M. Hasegaw, *Appl. Surf. Sci.*, 466, (2019) 837-846.

[12] M. Ghali, C. Brahmi, M. B. C. Vaultot, A. Airoudj, P. Fioux, F. Dumur, Corine S. Jégat, F. M. Savary, S. Jellali, L. Bousselmi, J. Lalevée, *J. Polym. Sci.* 59(2021) 153-169.

[13] X. Lin, Y. H. Wu, L. Y. Tang, M. H. Yang, D. Y. Ren, J. W. Zha, Z. M. Dang, *J. Appl. Polym. Sci.* (2016) 4308

[14] G. Balakrishnan, R. Velavan, Khalid Mujasam Batoo, Emad H. Raslan, *Results in Physics* 16 (2020) 103013

[15] Z. X. Tang, B. F. Lv, Braz, *J. Chem. Eng.* 31(2014) 591-601

[16] Y. Cai, D. Wu, X. Zhu, W. Wang, F. Tan, J. Chen, X. Qiao, X. Qiu, *J. Ceram. Int.* 43(2016) 1066-1072

[17] M. Moradia, G. Moussavia, K. Yaghmaeian, A. Yazdanbakhsh, V. Srivastavad, M. Sillanp, *J. App. Cat. B: Env.* 260 (2020) 118128

[18] M. Ghashghae, S. Shirvani, M. Ghambarian, *J App. Cat. A: Gen.* 545(2017) 134-147

[19] E. R. Essien, V. N. Atasi, A. O. Okefor, D. O. Nwude, *Nano Letters*, 10(2020) 43-48.

[20] N. Siddiqui, B. Sarkar, C. Pendem, R. Khatun, L. N. Sivakumar Konthala, T. Sasaki, A. Bordoloia, R. Bal, *Catal. Sci. Technol.* 7 (2017) 2828-2837

[21] D. Zhu, L. Wang, W. Yu, H. Xie, *Sci. Rep.* 8 (2018) 5282.

[22] N. F. Chayed, N. Kamarulzaman, N. Badar, K. Elong, *J. Solid State Phenomena* 290(2019) 323-328

[23] T. Linda, S. Muthupoongodi, X. Sahaya Shajan, S. Balakumar, *J. Mat. Sci. Forum.* 807(2015) 91-99.

[24] J. K. Vij (Eds), *Advances in Liquid Crystals, Advances in Chemical Physics*, John Wiley & Sons, pp. 259-261.

[25] G. Balakrishnan, R. Velavan, K. M. Batoo, E. H. Raslan, *J. Results in Physics* 16 (2020) 103013.

[26] N. C. S. Selvam, R. T. Kumar, L. J. Kennedy, J. Judith Vijaya, *J. Alloys Compd.* 509(2011) 9809-9815

- [27] K. Mageshwari, S. S. Mali, R. Sathyamoorthy, P. S. Patil, *J. Pow. Tech.* 249(2013) 456-462.
- [28] F. Mohandes, F. Davar, M. Salavati-Niasari, *J. Phys. Chem. Solids* 71(2010) 1623-1628.
- [29] N. Kamarulzaman, M.F. Kasim, N.F. Chayed, *J. Results in Physics* 6(2016) 217-230.
- [30] A/ M. El Sayed, *Mater. Res. Express.* 5 (2018) 116403
- [31] R. AME, J. VB, C. Ravidhas, T. Som, M. Jayachandran, C. Sanjeeviraja, *J. Rad. Phys. Chem.* 78 (2009) 914-921.
- [33] D. Wang, L. Shi, Q. Luo, X. Li, *Jing An, J. Mater Sci* 47(2012) 2136-2145.
- [34] P. Peerakiatkhajorn, C. Chawengkijwanich, W. Onreabroy, S. Chiarakorn, *J. Mat. Sci. Forum* 712 (2012) 133-145.

- [35] H. J. Lin, T. S. Yang, C. S. Hsi, M. C. Wang, K. C. Lee, *J. Ceram. Int.* 40 (2014) 10633–10640.
- [36] F. Bensouici, M. Bououdina, A. Dakhel, R. Tala-Ighil, M. Tounane, A. Iratni T. Souier S. Liu W. Cai, *App. Sur. Sci.* 395 (2016) 110-116
- [37] S. Abbas, B. Uzair, S. Sajjad, S.A.K. Leghari, S. Noor, M.B.K. Niazi, I. Farooq, H. Iqbal, *Arab. J. for Sci. Eng.* 47, (2021) 5895-5909
- [38] N. Rouabah, B. Boudine, R. Nazir, M. Zaabat, A.S. Alqahtani M.S. Alqahtani, R. Syed, *J. Poly. Res.* 28(2021) 154.